Electronic Supplementary Information

Sn@Ni_3Sn_4 embedded in nanocable-like carbon hybrids for stable lithium-ion batteries

Xiaoyu Hou [a], Yanjie Hu*[a] , Hao Jiang [a], Yunfeng Li[a,b], Xiaofeng Niu [a] and Chunzhong Li*[a]

[a] Key Laboratory for Ultrafine Materials of Ministry of Education, School of Materials Science and Engineering, East China University of Science & Technology, Shanghai 200237, China

[b] Shanghai Nanotechnology Promotion Center, Shanghai 200237, China

*To whom correspondence should be addressed.

E-mail: czli@ecust.edu.cn (Prof. C. Z. Li) and huyanjie@ecust.edu.cn (Dr. Y. J. Hu)

Fax: +86 21 64250624; Tel: 86- 21- 6425- 0949;

Experimental Section

1.1 Synthesis of $Sn@Ni_3Sn_4/C$ hybrids

1.1.1 FSP process

In a typical FSP experiment, 0.5 mol/L $SnCl_4 \cdot 5H_2O$ and $Ni(NO_3)_2 \cdot 6H_2O$ (molar ratio 2:1) dissolved in pure ethanol (100 mL) were employed as precursor solution. The precursor solution was fed at 5 ml/min through a spray nozzle and dispersed by external 5 L/min O_2 forming fine spray with a diffuse pressure of 0.15 MPa. Then the spray was ignited and reacted in the flame high temperature zone. The combustion atmospheres were controlled by adjusting the flammable gas flow of 0.38 m^3/h H_2 and the assisted-oxide gas flow of 1.5 m^3/h Air. The fresh productions were collected by glass fibers filter (ADVTECH/GA55, Toyo Roshi Kaisha Ltd. Japan) in the downstream of FSP equipment with the aid of vacuum pump.

1.1.2 CVD process

In a typical CVD experiment, 0.2 g SnO_2/NiO powders were put into furnace. The furnace temperature was heated to 650 ^oC for 2h with heating rate of 5 ^oC/min. The atmosphere was composed of 0.6 L/min 99.99% Ar and 30 mL/min C_2H_2. After cooling down to the room temperature, the final products were obtained.

1.2 Characterizations

The samples were characterized by Field emission scanning electron microscopy (FE-SEM: HITACHI S-4800) with energy dispersive X-ray spectroscopy (EDS), Transmission electron microscope (TEM: JEOL JEM-1400), High resolution Transmission electron microscope (HRTEM: JEOL JEM-2100), X-ray diffraction (XRD: D/max 2550V) and Thermogravimetric Analysis (TG: NETZSCH STA409PC). Nitrogen adsorption–desorption (ASAP 2010N) was determined by the Brunauer–Emmett–Teller (BET) method. X-ray photoelectron spectroscopy (XPS) experiments were carried out by Thermo Fisher (ESCALAB 25). The Raman spectrum (Raman) was characterized by Renishaw inVia/Reflex.

1.3 Electrochemical measurements

The working electrode was composed of active materials ($Sn@Ni_3Sn_4/C$ hybrids), conductive material (acetylene black, AB) and binder (polyvinyldifluoride, PVDF) with a weight ratio of 80:10:10. The three components were stirred into slurry with assistance of N-methyl-2-pyrrolidone

(NMP) and uniformly pasted on Cu foils (19 μm) with a controllable membrane thickness of 50 μm. Thin Li foils (φ16×1.2 mm) and polypropylene membrane (Celgard 2400) were employed as the counter electrode and separator, respectively. The electrolyte was 1 M $LiPF_6$ dissolved in ethylene carbonate/diethyl carbonate (EC-DEC, 1:1 w/w). The half-cells (CR2016 coin type) were employed and assembled in a high-purity argon filled glove box (Mikrouna Advanced Series) where moisture and oxygen levels were under 1 ppm. Cyclic voltammograms (CV) and electrochemical impedance spectroscopy (EIS) of the working electrode had been characterized by electrochemical workstation (Autolab PGSTAT302N). Galvanostatic cycle perfomance of coin cells were tested using on a LAND-CT2001C test system at several different current densities (from 100 mA h g^{-1} to 2000 mA h g^{-1}) in the voltage range from 0.01 V to 2.5 V.

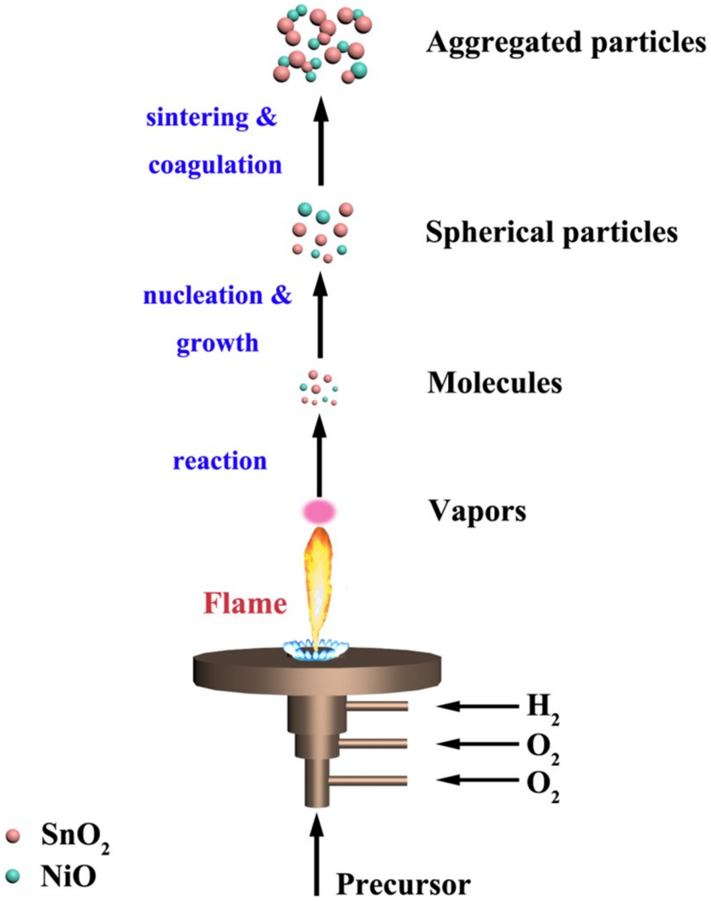

Figure S1. Schematic diagram of FSP route for preparation of SnO_2/NiO

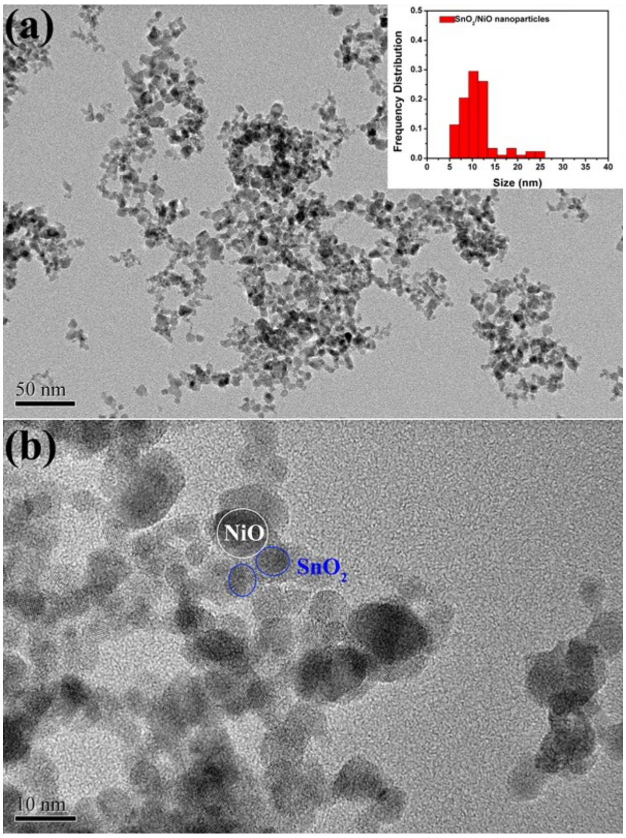

Figure S2 (a) TEM and (b) HRTEM of SnO$_2$/NiO nanoparticles made by FSP (inset of S1a was particle size distribution)

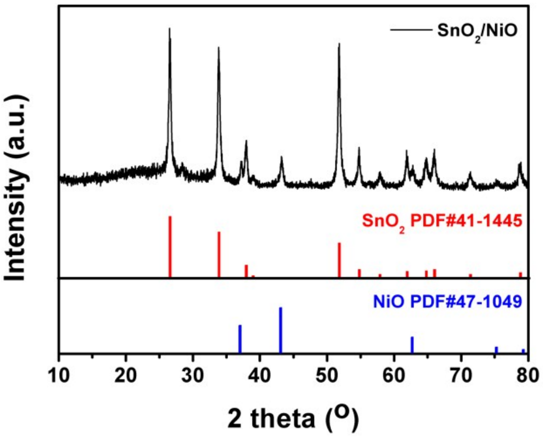

Figure S3 XRD pattern of flame-made SnO$_2$/NiO

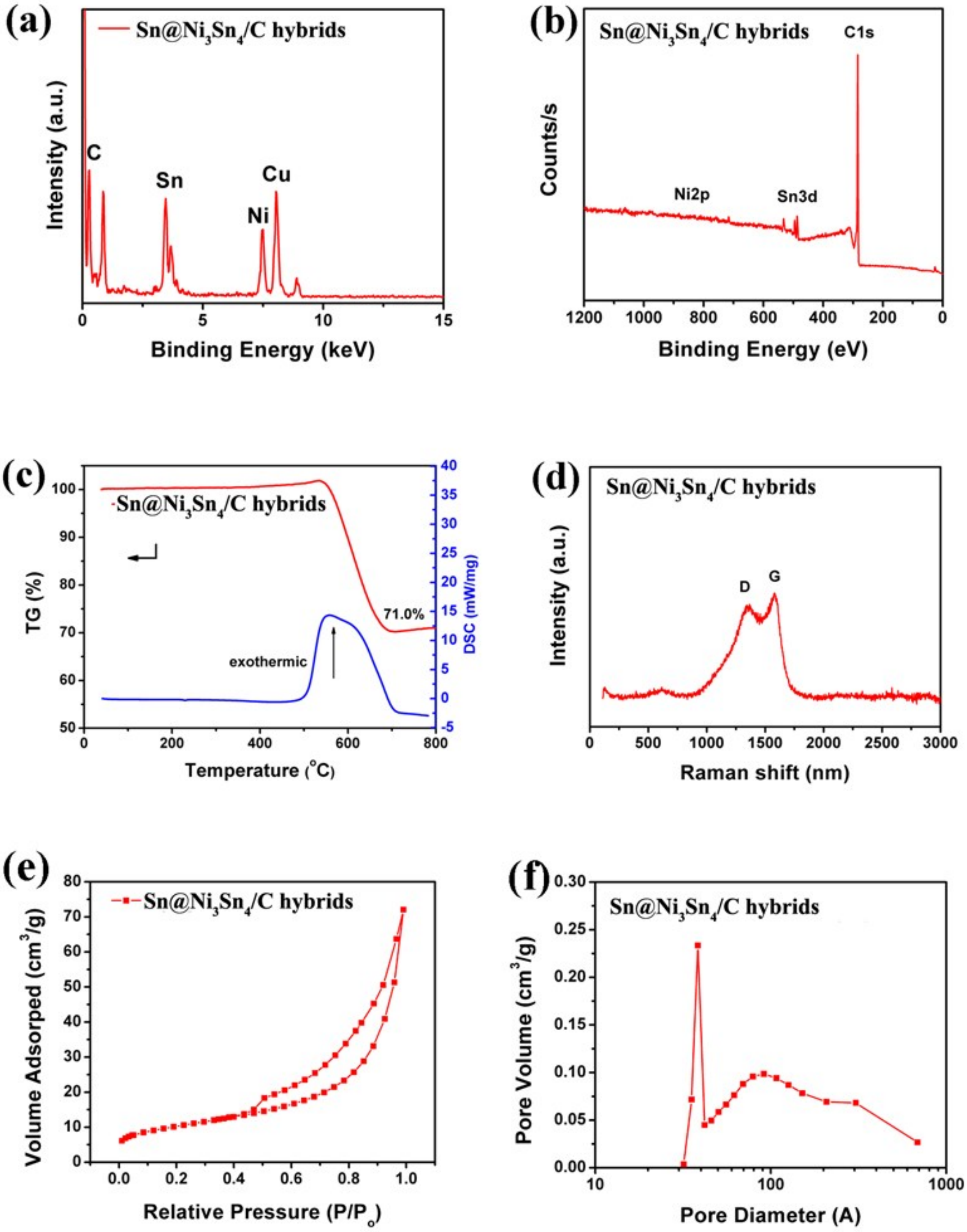

Figure S4. (a) EDS, (b) XPS, (c) TGA/DSC, (d) Raman, (e) BET, (f) Pore size distribution of $Sn@Ni_3Sn_4/C$ hybrids

Selected area EDS affirmed that no trace of O was found, ensuring no existence of metal oxides (Fig. S4a). The X-ray photoelectron spectroscopy (XPS) spectrum of the $Sn@Ni_3Sn_4/C$ hybrids was studied, further confirming the existence of Sn, Ni and C elements, and the valence of Sn and Ni was 0 (484.7 eV for 3d5/2 of metal Sn, 852.2 eV for $2p_{3/2}$ of metal Ni), which matched the metal state of Sn and intermetallic state of Ni_3Sn_4 (Fig. S4b). The carbon content of the as-prepared sample was calculated to be 44.0% by thermogravimetric analysis (TGA) (Fig. S4c). The Raman spectrum showed that I(D)/I(G) was equal to 0.9, indicating that the nanocable carbon layers had many defects (Fig. S4d). Besides, adsorption–desorption isotherms were carried out and the BET surface area of the $Sn@Ni_3Sn_4/C$ hybrids was 36.1 $m^2\ g^{-1}$ with a bimodal pore size distribution of 3.8 nm and 9.1 nm (Fig. S4e and f).

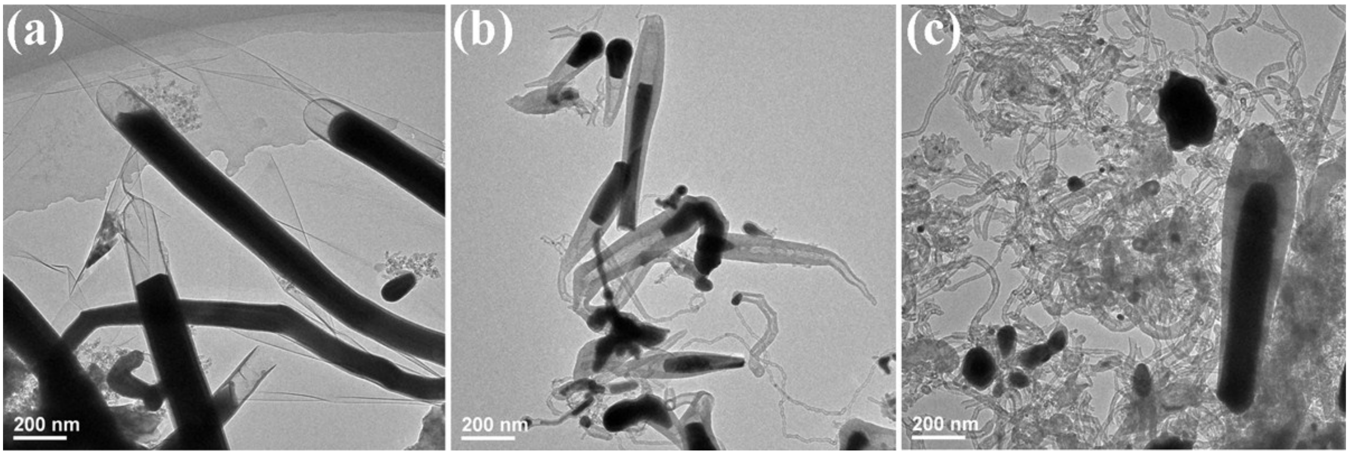

Figure S5 TEM images of (a) Sn@C nanowires catalayzed by SnO_2, (b) $Sn@Ni_3Sn_4/C$ hybrids catalyzed by sintered SnO_2/NiO, (c) Sn/C nanocomposites catalyzed by mixed of SnO_2 and NiO nanoparticles.

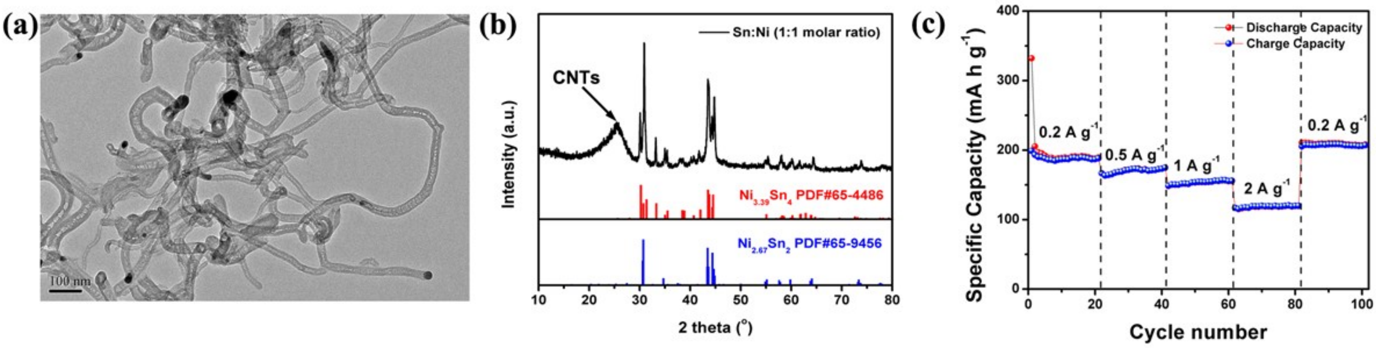

Figure S6 (a) TEM; (b) XRD (c) rate performance of contrast sample with Sn/Ni in 1:1 ratio.

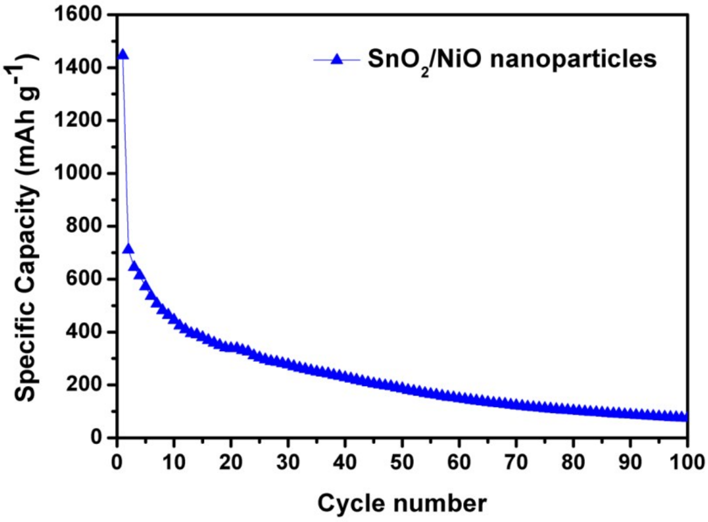

Figure S7. Cycling performance of flame-made SnO_2/NiO nanoparticles in the current density of 0.2

A g^{-1}.

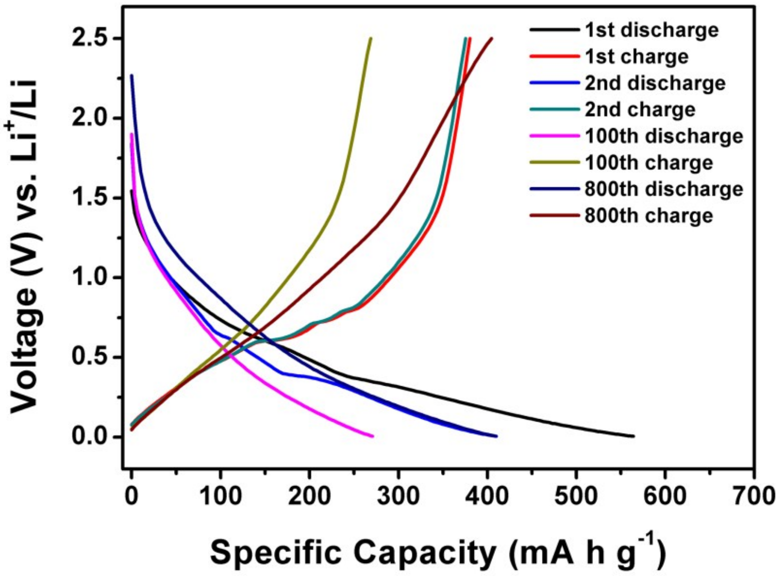

Figure S8. Charge/discharge *vs.* voltage of Sn@Ni_3Sn_4/C hybrids electrode

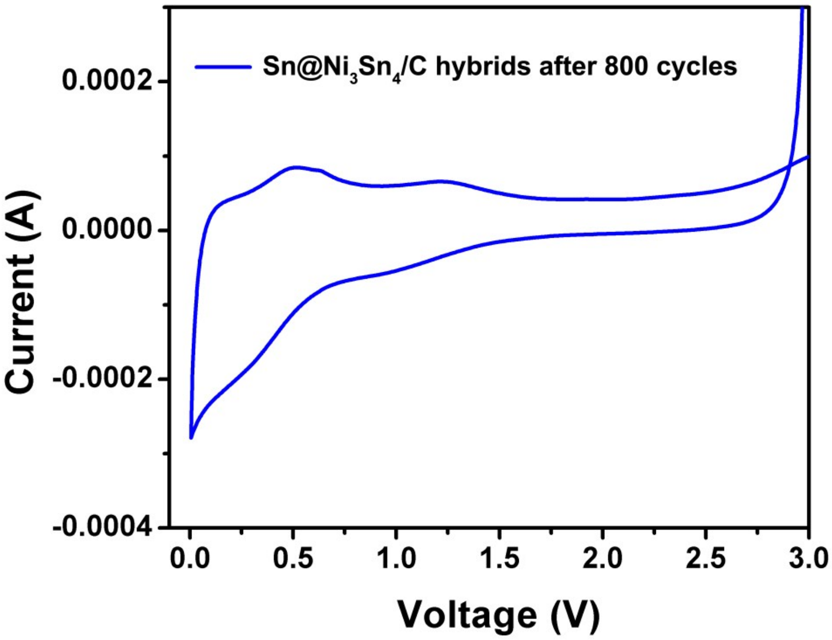

Figure S9. CV curve of Sn@Ni_3Sn_4/C hybrids electrode after 800 cycles.

The CV curve of the cell after 800 cycles had been tested to identify the electrochemical process after cycling, as shown in Fig. S9. Two separated broad peaks around 0.4–0.7 V and 1.1–1.3 V were ascribed to the characteristic peaks of deintercalation of Li_xSn and Li_yC, respectively, revealing that the capacity was still attributed to Sn and the carbon layer.